

# Adaptive Multi-Scale Computational Modeling of Composite Materials

P. Raghavan<sup>1</sup> and S. Ghosh<sup>2</sup>

**Abstract:** This paper presents an adaptive multi-level computational model that combines a conventional displacement based finite element model with a microstructural Voronoi cell finite element model for multi-scale analysis of composite structures with non-uniform microstructural heterogeneities as obtained from optical or scanning electron micrographs. Three levels of hierarchy, with different resolutions, are introduced in this model to overcome shortcomings posed by modeling and discretization errors. Among the three levels are: (a) level-0 of pure macroscopic analysis; (b) level-1 of macro-micro coupled modeling, used for signaling the switch over from macroscopic analyses to pure microscopic analyses; and (c) level-2 regions of pure microscopic modeling. The adaptive Voronoi cell finite element model is utilized effectively for analysis of extended microstructural regions with high efficiency and accuracy. Identification of statistically equivalent RVE (SERVE) for evaluating the effective properties are made through the use of correlation functions for different variables. Upon determination of SERVE's for actual microstructures, numerical examples of a composite plate and a composite laminate are solved to demonstrate the ability of the multi-scale computational model in analyzing complex heterogeneous structures.

**keyword:** Voronoi cell FEM, multi-scale analyses, non-uniform microstructures

## 1 Introduction

The commercial use of reinforced composites in various structural components has increased considerably in the last few decades. Based on design requirements, they are engineered to yield superior thermo-mechanical properties like high strength or stiffness to weight ratios, resulting in a tremendous advantage over monolithic ma-

terials. Despite property enhancements, the presence of second phase fibers or particles in composites often has adverse effects on their failure properties like fracture toughness and strain to failure. Structural components, e.g. laminates of many composite materials, exhibit strong non-uniformities at the microstructural level. The non-uniformities are in micro-scale morphology including variable fiber/particle spacing, size, shape, volume fraction and dispersion, in meso-scale clustering or directionality or in varying constituent material and interface properties. The material response and especially microstructural damage mechanisms, including inclusion and matrix cracking, interfacial decohesion etc. can be very sensitive to these local variations in morphological and constitutive parameters. Robust analysis methods to design optimal composite microstructures are necessary for enhanced utilization of composite materials in load bearing high performance applications.

Heterogeneous structures are conventionally analyzed with properties obtained from homogenization of response at smaller (meso-, micro-) length scales. [Ghoniem and Cho (2002)] provides an overview of current and a vision for future developments in multiscale simulations for nano- and micro-mechanics of materials. Analysis of composite materials is often performed by the method of homogenization wherein the macroscopic properties are obtained by averaging stresses and strains over a periodic representative volume element (RVE). Commonly used methods of homogenization, e.g. the asymptotic expansion homogenization [Bensoussan, Lions and Papanicolau (1978); Sanchez-Palencia (1980)], assume spatial periodicity of microstructural representative volume elements or RVE's and uniformity of macroscopic variables. Multiple scale analyses of linear elastic reinforced composites have been conducted by Fish et. al. [Fish and Wagiman (1993)], Guedes and Kikuchi [Guedes and Kikuchi (1991)], Ghosh et. al. [Ghosh, Lee and Raghavan (2001); Raghavan, Moorthy, Ghosh and Pagano (2001)]. In this issue, the homogenization method has

---

<sup>1</sup> Graduate Research Associate

<sup>2</sup> Professor, Department of Mechanical Engineering, The Ohio State University, Columbus, Ohio, USA

been used in conjunction with the boundary element method for three-dimensional particle reinforced composites in [Okada, Fukui and Kumazawa (2003)]. Micromechanical traction-displacement laws are embedded in the continuum macromechanical formulation by a variational multiscale method in [Garikipati (2002)]. The application of homogenization methods suffer from some shortcomings with respect to accuracy in specific problems with respect to limitations in the assumptions of macroscopic uniformity and RVE periodicity. The uniformity assumption is not appropriate in critical regions of high gradients like free edges [Pagano and Rybicki (1974); Rybicki and Pagano (1976); Raghavan, Moorthy, Ghosh and Pagano (2001)], interfaces, material discontinuities and most importantly in regions of evolving damage. Periodicity of simple unit cells is also unrealistic for non-uniform microstructures, particularly in the presence of clustering. Even with uniform distribution of microstructures, evolving localized stresses or strains can violate the periodic assumptions. Problems like this have been tackled effectively by global-local techniques introduced by Fish et. al. [Fish and Wagiman (1993)], Ghosh et. al. [Ghosh, Lee and Raghavan (2001); Raghavan, Moorthy, Ghosh and Pagano (2001)] and Oden et. al. [Oden and Zohdi (1997)]. Sub-structuring in these multiple-scale analysis methods differentiate between regions requiring different resolutions, and enable global analysis in some parts of the domain and zoom in for complete microscopic modeling at region of high gradients. Adaptivity is a desirable ingredient of these multiple scale modeling methods, for automatically selecting appropriate regions to minimize discretization and modeling errors. Without adaptivity, hierarchical modeling may not be optimally efficient. Adaptive multiple-level methods have been proposed by Oden et. al. [Oden and Zohdi (1997); Oden, Vemaganti and Moes (1999)], Ghosh et. al. [Ghosh, Lee and Raghavan (2001); Raghavan, Moorthy, Ghosh and Pagano (2001)] to address discretization and modeling error for multi-scale analysis of composites.

A second shortcoming of composite analysis using the asymptotic homogenization methods is related to efficiency in the concurrent execution of finite element analyses at the macroscopic and microscopic scales. Enormous computational efforts can result from having to solve boundary value problems of the microstructural RVE in each macroscopic element of a finite element

model, in addition to the macroscopic solution. To economize computations, many studies have assumed simple unit cells models of the RVE, consists of a rectangular domain with one or two fibers. These simplified RVE's often imply uniform or hexagonal closed-pack distributions in the microstructure bearing little resemblance with the actual stereographic features of the actual microstructure. Multiple scale models incorporating the Voronoi cell microstructural models have proved to possess significant edge in this regard. The microstructural Voronoi Cell Finite Element Model (VCFEM) has been developed by Ghosh et. al. [Moorthy and Ghosh (1996, 1998, 2000); Ghosh, Ling, Majumdar and Kim (2000)] to overcome limitations of unit cell models and effectively analyze large microstructural regions with arbitrary dispersions, shapes and sizes of heterogeneities. By combining assumed stress hybrid finite element formulations with essential characteristics of micromechanics, a high level of computational efficiency with good accuracy and resolution has been achieved with this method. In this issue a 3D model for stress and damage analysis in multi-inclusion discontinuously reinforced composites has been proposed by Böhm et. al. [Böhm, Han and Eckschlager (2003)] and a model for woven fabric composites has been proposed by Kwon and Roach [Kwon and Roach (2003)].

While VCFEM offers a solution to efficient analysis of complex microstructures, identifying statistically equivalent representative volume elements or SERVE for non-uniform microstructures is a challenge. Underrepresentation of SERVE's can lead to considerable errors in the values of effective properties and should be avoided. Various authors have used statistical analyses to determine the size scale of RVE and the number of fibers contained in it [Pyrz (1994a,b), Bulsara, Talreja and Qu (1999)]. Pyrz et. al. [Pyrz (1994a,b)] has used statistical correlation functions to obtain characteristic information about the microstructure. For example, geometric descriptors like the second order intensity function and pair distribution functions have been used to distinguish between different patterns or distributions. To account for the interaction between fibers, they have used the marked correlation function as an informative descriptor for characterizing the size of the microstructural SERVE. The marked correlation functions combines both the geometric descriptors as well as distributions of response variables like stresses and strains in the microstructure.

In this paper, a systematic multi-scale analysis method is established for fiber reinforced composite structures consisting of non-uniformly dispersed microstructures. The multi-level computational model introduced in [Ghosh, Lee and Raghavan (2001); Raghavan, Moorthy, Ghosh and Pagano (2001); Lee, Moorthy and Ghosh (1999)] for simple microstructures is extended in this work. The model encompasses three levels in the computational domain. The level-0 and level-1 subdomains use effective properties obtained by homogenization of the statistically equivalent RVE's, obtained using marked correlation functions in the microstructure. Unique methods of applying periodic boundary conditions on non-uniform RVE's are developed. Level-2 sub-domains emerge with loss of periodicity or uniformity in macroscopic regions, where the model switches to complete microscopic calculations using precise microstructures. Details of the multiple scale computational model is provided in Section 4. Numerical examples demonstrating the effectiveness of the model are provided in Section 7.

## 2 The Asymptotic Expansion Homogenization Method

Boundary value problems in a heterogeneous domain  $\Omega^\varepsilon$  are assumed to satisfy the equations of linear elasticity, given as

$$\text{Equilibrium} : \quad \sigma_{ij,j}^\varepsilon = -f_i$$

$$\text{Kinematics} : \quad e_{kl}^\varepsilon = \frac{1}{2} \left( \frac{\partial u_k^\varepsilon}{\partial x_l^\varepsilon} + \frac{\partial u_l^\varepsilon}{\partial x_k^\varepsilon} \right)$$

$$\text{Constitutive Relations} : \quad \sigma_{ij}^\varepsilon = E_{ijkl}^\varepsilon e_{kl}^\varepsilon \quad \text{in } \Omega^\varepsilon \quad (1)$$

where  $\sigma_{ij}^\varepsilon$ ,  $e_{ij}^\varepsilon$  and  $u_i^\varepsilon$  are stress, strain and displacement fields respectively. The scale parameter  $\varepsilon = \frac{l_y}{l_x}$  ( $l_y, l_x$  correspond to length scales in the microscopic and macroscopic domains respectively) is typically an infinitesimally small number. Since computational analysis of this problem will be prohibitively expensive due to the presence of large number of heterogeneities, most analysts solve an equivalent homogenized version of the problem using macroscopic effective properties obtained by averaging microscopic variables. A powerful method that has been developed in conjunction with computational analysis of heterogeneous materials is the asymptotic expansion homogenization method [Benssousan, Lions and Papanicoulau (1978); Sanchez-Palencia (1980)]. In this method variables (stresses, strains and displacements)

are assumed to exhibit dependence on the macroscopic as well as microscopic length scales. Furthermore, the microscopic dependence is assumed to be  $Y$ -periodic, where  $Y$  is the period of RVE. In this method, the displacement field in a heterogeneous domain is expanded asymptotically about its values at a macroscopic point  $\mathbf{x}$ , in terms of the microscopic coordinates  $\mathbf{y}$  as

$$u_i^\varepsilon(\mathbf{x}) = u_i^0(\mathbf{x}, \mathbf{y}) + \varepsilon u_i^1(\mathbf{x}, \mathbf{y}) + \varepsilon^2 u_i^2(\mathbf{x}, \mathbf{y}) + \dots, \quad \mathbf{y} = \frac{\mathbf{x}}{\varepsilon} \quad (2)$$

The spatial derivative of any multi-scale function is given as

$$\frac{\partial}{\partial x_i^\varepsilon} (\Phi(\mathbf{x}, \mathbf{y})) = \frac{\partial \Phi}{\partial x_i} + \frac{1}{\varepsilon} \frac{\partial \Phi}{\partial y_i} \quad (3)$$

Using Eq. 2 and Eq. 3 in kinematics and constitutive relations of Eq. 1 yields the stress tensor  $\sigma_{ij}^\varepsilon$  as

$$\sigma_{ij}^\varepsilon = \frac{1}{\varepsilon} \sigma_{ij}^0 + \sigma_{ij}^1 + \varepsilon \sigma_{ij}^2 + \varepsilon^2 \sigma_{ij}^3 \dots \quad (4)$$

Using Eq. 3 and Eq. 4 in the equilibrium relation of Eq. 1, equating various powers of  $\varepsilon$  and averaging over the periodic RVE, it can be shown that the following relations hold.

$$\begin{aligned} u_i^0 &= u_i^0(\mathbf{x}) \\ \sigma_{ij}^0 &= 0 \\ u_i^1 &= \chi_i^{kl}(\mathbf{y}) \frac{\partial u_k^0}{\partial x_l} \\ \sigma_{ij}^1 &= \hat{\sigma}_{ij}^{kl}(\mathbf{y}) \frac{\partial u_k^0}{\partial x_l} \end{aligned} \quad (5)$$

where  $\hat{\sigma}_{ij}^{kl}$ ,  $\chi_p^{kl}$  are the microscopic stresses and characteristic deformation modes. Furthermore the volume average of microscopic stresses yields the homogenized stiffness tensor  $E_{ijkl}^H$  for use in macroscopic calculations.

$$\begin{aligned} E_{ijkl}^H &= \langle \hat{\sigma}_{ij}^{kl} \rangle_Y = \frac{1}{|Y|} \int_Y \hat{\sigma}_{ij}^{kl} dY \\ &= \frac{1}{|Y|} \int_Y E_{ijpnm}^\varepsilon (\delta_{kp} \delta_{lm} + \frac{\partial \chi_p^{kl}}{\partial y_m}) dY \end{aligned} \quad (6)$$

The macroscopic stress-strain relation then takes the form

$$\Sigma_{ij}(\mathbf{x}) = \langle E_{ijkl}^\varepsilon (\delta_{km} \delta_{ln} + \frac{\partial \chi_k^{mn}}{\partial y_l}) \frac{\partial u_m^0}{\partial x_n} \rangle_Y = E_{ijmn}^H e_{mn}(\mathbf{x})$$

(7)

where the homogenized variables are  $\Sigma(\mathbf{x}) = \langle \sigma^\varepsilon(\mathbf{x}, \mathbf{y}) \rangle_Y$  and  $\mathbf{e}(\mathbf{x}) = \langle e^\varepsilon(\mathbf{x}, \mathbf{y}) \rangle_Y$ . The components of the homogenized stiffness matrix  $E_{ijkl}^H$  are calculated by detailed solution of separate boundary value problems of the entire RVE. The loading in each of these problems is in the form of imposed unit macroscopic strains. Additionally, the periodicity on RVE boundaries implies that points on the boundary are constrained to displace periodically. For nodes on the boundary which are separated by the periods  $Y_1, Y_2, Y_3$  along one or more coordinate directions, the displacement constraints can be expressed as

$$u_i(x_1, x_2, x_3) = u_i(x_1 \pm k_1 Y_1, x_2 \pm k_2 Y_2, x_3 \pm k_3 Y_3), \quad (8)$$

$$i = 1, 2, 3$$

where  $k_1, k_2, k_3$  may assume the values 0 or 1, depending on the node locations.

### 3 Estimating Statistically Equivalent RVE's for Non-uniform Microstructures

Macroscopic analysis of a composite structure, requires that an appropriate RVE be identified for each macroscopic point. RVE's can be readily identified for a regular arrangement of fibers like rectangular or hexagonal distributions. However, microstructures from real composite materials hardly possess regular distribution as shown in Fig. 1(b). In Fig. 1 a composite plate with a circular hole and the corresponding microstructure from a optical micrograph are shown. The fibers are assumed to be aligned perpendicular to the plane of paper. Since this microstructure is random, a RVE can be obtained only in a statistical sense and attention is focused on identifying a Statistically Equivalent RVE (SERVE), which would exhibit a macroscopic behavior that is equivalent to the average behavior of the corresponding microstructure.

The microstructure shown in Fig. 1(b) corresponds to macroscopic point A only. Since the construction of SERVE's for the entire plate would require a large number of micrographs from various representative points in the plate, an assumption is made that, this is a representative microstructure for the entire plate. This may be justified from two considerations from statistical continuum theories that have been described in [Beran (1968)], viz. (a) an ensemble assumption, in which different experiments with different microstructural arrangements exhibit similar macroscopic behavior, and (b) an ergodic

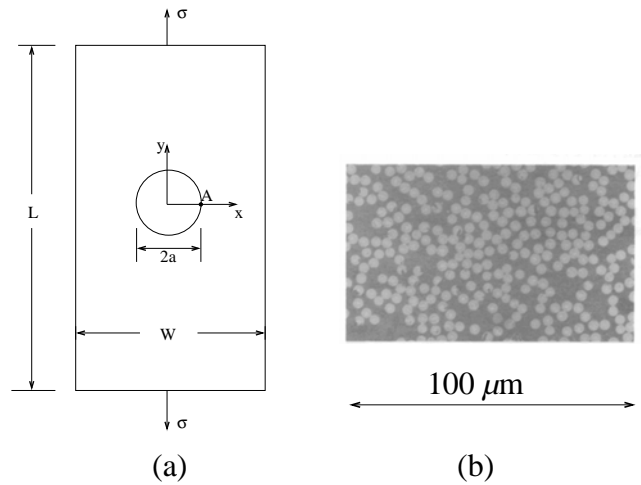


**Figure 1 :** (a) Composite plate with a hole (b) Optical micrograph of the microstructure at point A

hypothesis, which demands that all states available to ensemble of systems be available to each system of the ensemble. The justification of the assumptions have been provided in [Zeman and Sejnoha (2001)]. Consequently a single SERVE is assumed to represent every macroscopic point in the plate. The representative size of the SERVE is identified by the use of statistical functions, e.g. correlation functions. Pyrz [Pyrz (1994b)] has introduced “marked correlation functions” for characterizing the length scales defined as the region of influence in a heterogeneous neighborhood on pre-disposed response fields like stresses and strains. The marked correlation function for a heterogeneous domain of area  $A$  containing  $N$  fibers may be expressed as

$$M(r) = \frac{dH(r)}{g(r)} \quad (9)$$

where

$$H(r) = \frac{1}{m^2} \frac{A}{N^2} \sum_i^N \sum_{k=1}^{k_i} m_i m_k(r) \quad (10)$$

In the above equation  $m_i$  is a mark associated with  $i$ th fiber,  $k_i$  is the number of fibers which have their centers within a circle of radius  $r$  around the  $i$ th fiber,  $m_k$  are the marks of those fibers and  $m$  is the mean of all the marks. Marks in the marked correlation function can be any field variable for example, the maximum principal stress, Von Mises stress etc. associated with each fiber.

$H(r)$  is called the mark intensity function and  $g(r)$  is the pair distribution function defined as

$$g(r) = \frac{1}{2\pi r} \frac{dK(r)}{dr} \quad (11)$$

where  $K(r)$  is a second order intensity function which is explained in [Ghosh, Nowak and Lee (1997a,b)]. While  $K(r)$  can distinguish between different patterns, the pair distribution function  $g(r)$  characterizes the intensity of inter fiber distances. From the definition it can be seen that the marked correlation function associates field variables with morphology of the microstructure. The radius of influence  $R_{inf}$  may be inferred from a plot of  $M(r)$  vs  $r$ , in which  $M(r)$  stabilizes as  $r$  approaches  $R_{inf}$ .

Once the radius of influence  $R_{inf}$  has been determined from  $M(r)$ , SERVE may be constructed by using square windows of size  $R_{inf} \times R_{inf}$  at various points of the micrograph. The use of square windows to carve out the RVE for a random microstructure results in the intersection of many fibers with the edges yielding cut fibers near the boundary, as shown in Fig. 2(a). While some authors have used cut fibers in their RVE construction [Zeman and Sejnoha (2001)], the application of periodic boundary condition is improper with these RVE's. Increasing the window size to include the totality of cut fibers, as done in [Bulsara, Talreja and Qu (1999)] (Fig. 2(b)), results in a decreased volume fraction.

As a remedy, to the above discrepancies, a method of constructing the SERVE boundary by repeating the group of fibers periodically is adopted in this work as shown in Fig. 2(c).

The local microstructure is first constructed by repeating the randomly distributed fibers obtained from statistical analysis in both the  $y_1$ - and  $y_2$ - directions for several period lengths. Periodic repetitive fibers are placed at  $(y_1, y_2)$ ,  $(y_1 \pm k_1 Y_1, y_2)$ ,  $(y_1, y_2 \pm k_2 Y_2)$  and  $(y_1 \pm k_1 Y_1, y_2 \pm k_2 Y_2)$ , where  $k_1, k_2$  are integers. The period lengths  $Y_1$  and  $Y_2$  are selected such that the volume fraction of the RVE matches with that of the original microstructure. The multi-fiber domain is then tessellated into a network of Voronoi cells [Ghosh and Mukhopadhyay (1991)] as shown in Fig. 2(c). The boundary of the RVE, shown in bold lines, is generated as the aggregate of the outside edges of Voronoi cells associated with the primary fibers (dark colored). The consequent SERVE will have non-straight line edges corresponding to non-uniform fiber arrangements. However, nodes on the RVE

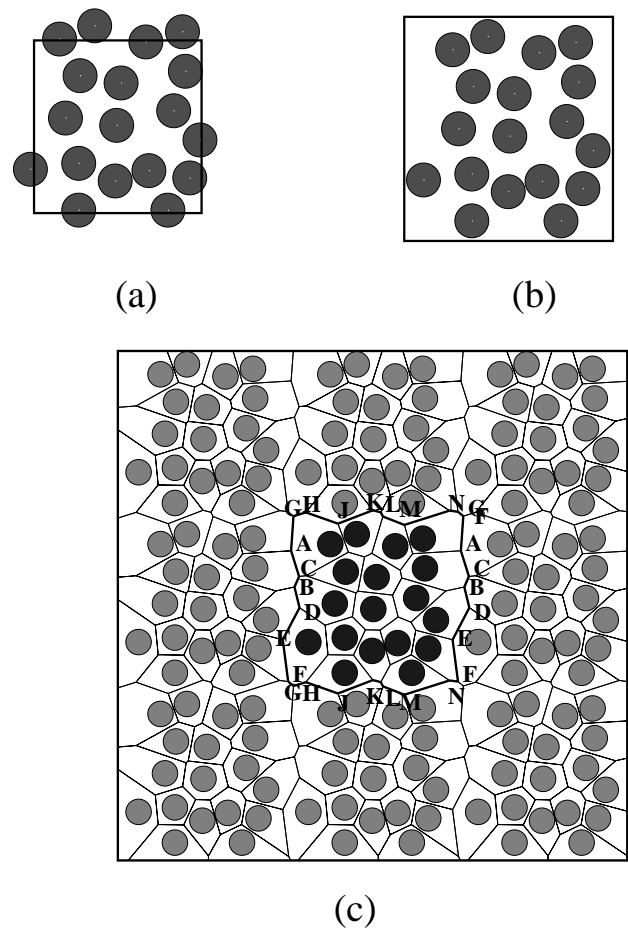


**Figure 2** : (a) Particles cut during the RVE generation (b) Boundary of the RVE adjusted to accommodate the complete particle (c) Construction of periodic RVE with non-straight edges

boundary, created by this procedure are periodic, i.e. for every boundary node a periodic pair can be identified on the boundary at a distance of one period along one or both of the coordinate directions. In Fig. 2(c), the node pairs are identified as AA, BB etc. The periodicity constraint conditions on nodal displacements can then be easily imposed.

### 3.1 Convergence in the Size of SERVE

A numerical example is used to demonstrate the effect of size of the constructed SERVE on the macroscopic properties as well as the microscopic stresses. The pair distribution function  $g(r)$  for the entire microstructure (Fig. 1) is evaluated and depicted in Fig. 3, where  $r_o$  is the fiber

radius. Instead of using a correction factor for evaluating  $K(r)$ , periodicity of the micrograph is used. A comparison with a pure random Poisson distribution ( $g(r) = 1$ ) shows that the microstructure considered exhibits significant deviation from randomness through clustering etc. High levels of clustering are seen for lower levels of  $r$  ( $< 8r_o$ ), and the clustering intensity decreases with increasing radial distance.

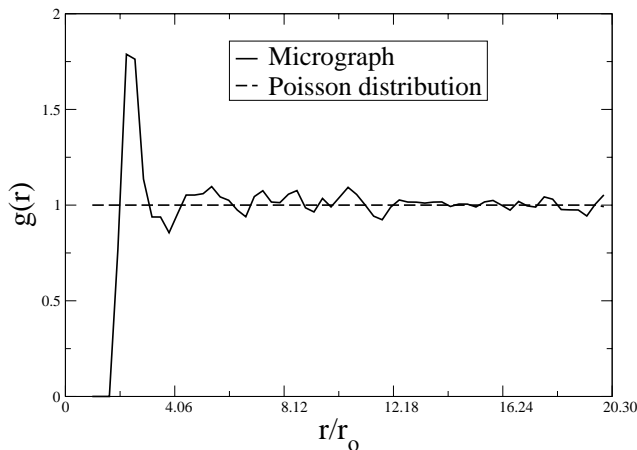
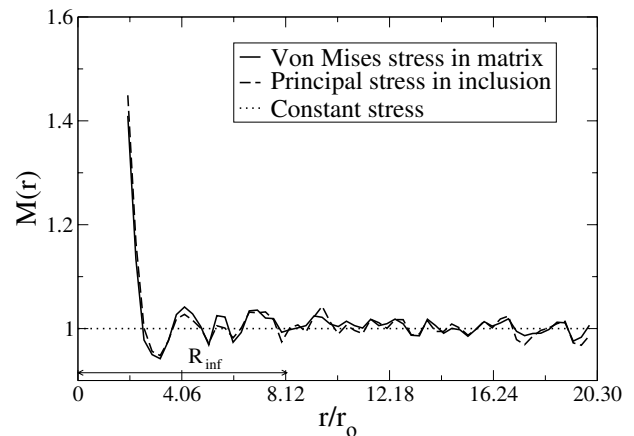
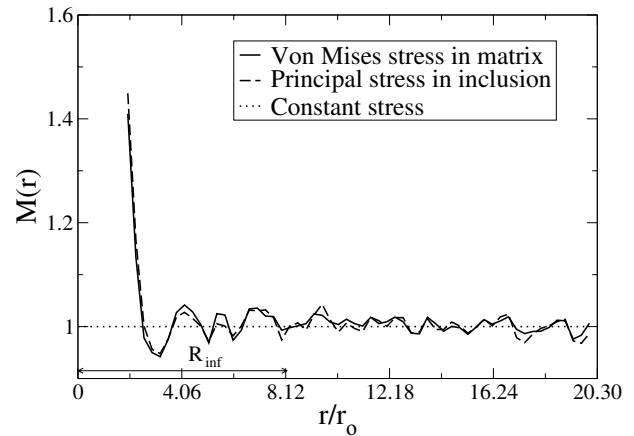


**Figure 3 :**  $g(r)$  distribution for the micrograph

Maximum principal stress in the fiber and maximum Von Mises stress in matrix in each Voronoi cell are considered as marks since they are good indicators of failure initiation in the microstructure. These variables are obtained by detailed computational analysis of the entire micrograph under tensile loading by the Voronoi Cell finite element method (VCFEM), described in Section 4.3, [Moorthy and Ghosh (1996)]. The VCFEM mesh is generated by tessellating the entire micrograph into a network of Voronoi cells [Ghosh and Mukhopadhyay (1991)]. Plots of  $M(r)$  for different marks are shown in Fig. 4(a). It can be seen that  $M(r)$  is high at distances less than  $8r_o$  but stabilizes to a unit value at distances greater than approximately  $8r_o$ . This indicates that the influence on the stress persists for fibers within an approximate radius of  $8r_o$ . It can also be seen that  $M(r)$  for both Von Mises stress and principal stress have a similar behavior and stabilize approximately in the same radial range. A very similar behavior of  $M(r)$  is also observed when the micrograph is loaded under biaxial tension as shown in Fig. 4(b). This suggests that a length of around  $8r_o$  can characterize the size scale of the statistically equivalent



(a)



(b)

**Figure 4 :** Marked correlation functions  $M(r)$  for (a) uniaxial loading and (b) biaxial loading

representative volume element.

Convergence in effective macroscopic moduli and microscopic stress distributions with respect to the RVE size is now studied. 5 different RVE's, shown in Fig. 5, are considered with periodic boundary conditions. They consist of 1, 8, 18, 35 and 55 fibers respectively with corresponding RVE sizes of  $r_o$ ,  $3r_o$ ,  $6r_o$ ,  $9r_o$  and  $12r_o$ . The RVE's are chosen from any arbitrary region (Region A) in the micrograph. The matrix material is assumed to be epoxy with properties  $E_m = 3.8$  GPa and  $\nu_m = 0.34$ , while the fibers are of graphite with properties  $E_f = 380.0$  GPa and  $\nu_f = 0.2$ . The effective properties are calculated by the homogenization method using Eq. 6. A Frobenius

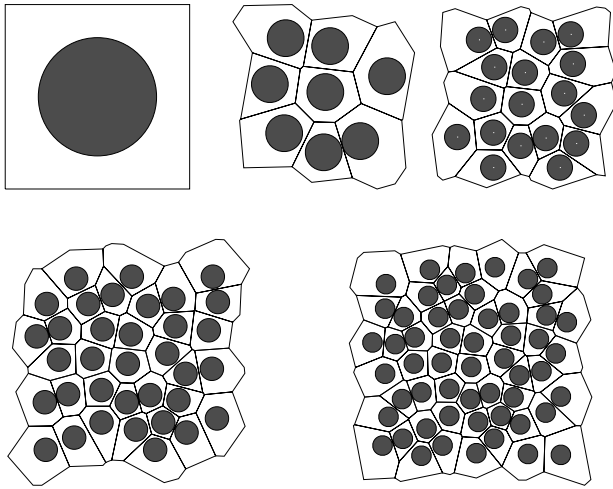


**Figure 5** : RVE's with 1, 8, 18, 35 and 55 fibers

norm of the effective elastic modulus is given as

$$\|E\| = \sqrt{\sum_{i=1}^N \sum_{j=1}^N E_{ij}^2} \quad (12)$$

where  $N = 3$  for plane stress and plane strain. Fig. 6 shows the convergence of  $\|E\|$  with the increasing RVE sizes. The norm converges with increasing RVE sizes. The difference in the norm between the single fiber and 55 fibers is around 2%, while the difference between 18 fibers (corresponding to  $R_{inf} = 10\mu\text{m}$  in Fig. 4) and 55 fibers is found to be less than 0.5%. Similar responses are observed for other regions (Region B) in the microstructure as shown with the dotted line in Fig. 6. Consequently, a size scale of  $r = 6r_o$  is deemed adequate for the SERVE to be used in all subsequent analyses.

In the study of the effect of RVE size on microscopic stresses, unit macroscopic strains  $e_{xx} = 1$ ,  $e_{yy} = 0$ ,  $e_{xy} = 0$ ,  $e_{zz} = 0$  are imposed on the RVE's with periodic boundary conditions. Fig. 7 shows the macroscopic stress ( $\Sigma_{xx}$ ), the maximum Von Mises stress in the matrix and the maximum principal stress in the fiber, as functions of increasing RVE size. While the macroscopic stress is almost insensitive to the RVE size, the maximum stresses in the microstructure change considerably. The difference in maximum Von Mises stress in the matrix for the single fiber RVE and 55 fiber RVE is almost 60% whereas, the corresponding difference for the 18 fiber RVE and the 55 fiber RVE is less than 4%. This

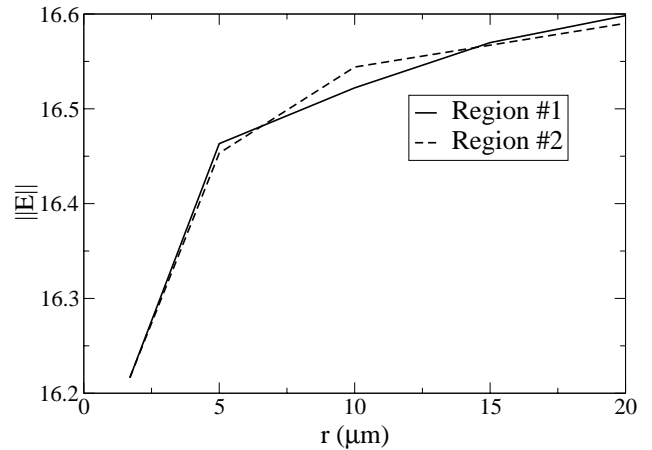


**Figure 6** : Convergence of  $\|E\|$  with increasing RVE sizes at different regions

study reasserts the effectiveness of the marked correlation function in determining the SERVE size.

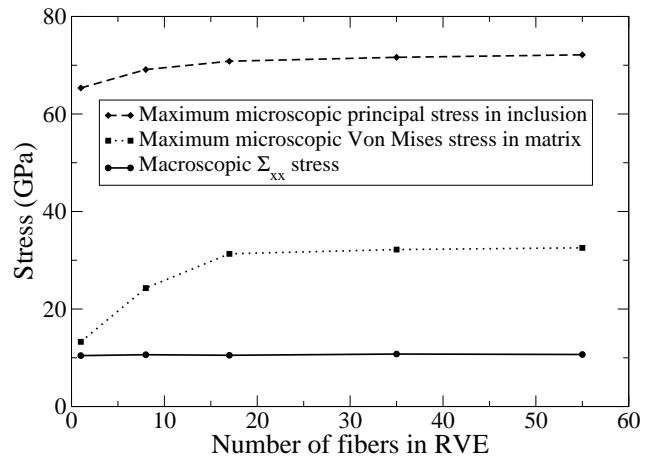


**Figure 7** : Convergence of macroscopic and microscopic stress for unit strain loading for different RVE sizes

#### 4 The Adaptive Multi-Scale Computational Model

Even if a RVE with a large number of heterogeneities is used, the microscopic stresses or strains at critical locations may be grossly misrepresented in purely macroscopic studies with effective moduli established through microscopic homogenization, due to the assumptions of periodicity and macroscopic uniformity associated with the definition of a RVE. It has been noticed by many

authors [Pyrz (1994a); Daniel and Anastassopoulos (1995)] that local morphology of fibers have strong effect on failure initiation and propagation. The multi-scale computational model has been developed in [Ghosh, Lee and Raghavan (2001); Raghavan, Moorthy, Ghosh and Pagano (2001)] to overcome the limitations of pure homogenization based analyses of heterogeneous materials. This model is adaptive in nature and automatically distinguishes between critical and non-critical regions to introduce levels of hierarchy in the computational model. In this paper, the model is extended to microstructures with non-uniform distribution of fibers. The main computational subdomains in the hierarchical model are shown in Fig. 8 and discussed next.

#### 4.1 Computational Subdomain Level-0

Level-0 subdomains encompass regions of macroscopic analysis using effective properties obtained by homogenization of SERVE. This level is valid in regions where macroscopic gradients in variables like stresses or strains are relatively small. For each element in the level-0 subdomain, a SERVE is identified and the asymptotic homogenization method is then used for obtaining effective material properties. Conventional displacement based elements are used for the level-0 element formulation. Each element stiffness matrix and load vector is evaluated and stored for global assembly for this subdomain.

#### 4.2 Computational Subdomain Level-1

Level-1 subdomains are intended as ‘transition’ regions, where microscopic information in the SERVE is used to decide whether microscopic computations are necessary for these regions. They are seeded in regions of locally increasing gradients of macroscopic variables in the pure level-0 simulations. These gradients may be caused by microscopic non-homogeneity in the form of large localized stresses and strains, or when the microstructure faces possible damage initiation or localization. Computations in this region are still based on assumptions of macroscopic uniformity and periodicity of the RVE. Concurrent with macroscopic simulations, computations are executed in the microstructure to monitor variables in the RVE. Computational requirements for microstructural analysis of elements in this level are considerably higher than that for level-0. It is therefore important to design robust criteria to avoid redundant element transition from level-0 to level-1. Major steps involved in

level-1 element computations are

- Setting up the macroscopic stiffness by solving RVE level boundary value problems with unit strains and periodic boundary conditions
- Post-processing to compute microscopic stresses in the RVE at each integration point of the macroscopic element

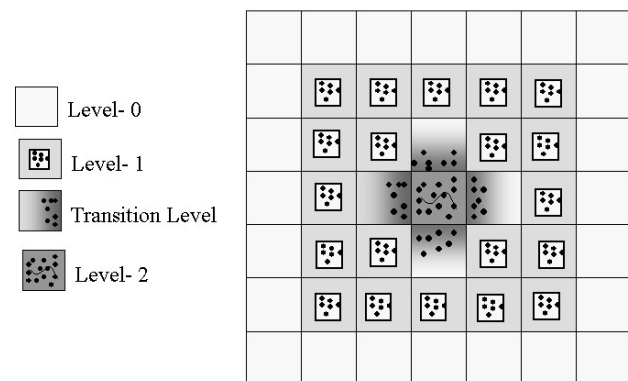


**Figure 8 :** Multi-level mesh showing different levels for the multi-scale model

##### 4.2.1 Adaptive Level-0 and Level-1 Mesh Enrichment

The discretization error in level-0 and level-1 are reduced by performing adaptive refinement to increase resolution in required regions of the model. Different types of adaptations are possible for these models. Three popular refinements viz., the  $h$ -version,  $p$ -version and the  $hp$ -version have been proposed in literature. The simple and most common is the  $h$ -version, where refinement is accomplished by subdividing the element while keeping the same polynomial order of the element. In the  $p$ -version, the size of an element is kept constant, but the order of interpolating polynomial is increased. In the  $hp$ -version both of the above refinements are included. When high accuracy is required, the use of  $p$ -version or the  $hp$ -version is necessary. Mathematical and numerical work by Babuska and co-workers [Babuska and Szabo (1991)], have shown that with the  $hp$ -refinement, it is possible to achieve an exponential rate of convergence to the exact solution for many problems, including those with singularities. The rate of convergence in the  $hp$ -

adaptive method has been estimated [Guo and Babuska (1986a,b)] as

$$\|u - u_{fe}^{hp}\| \leq C h^\mu p^{-(m-1)} \|u\| \quad (13)$$

where  $\mu = \min(p, m-1)$ ,  $p$  = polynomial order,  $m$  = regularity of the solution and  $C$  = constant independent of  $h$  and  $p$ . The estimate shows that the rate of convergence will be slow if  $m-1$  is less than  $p$ . On the other hand if  $m$  is large, which is the case when the solution is very smooth, the rate of convergence will be limited only by the order of polynomial  $p$ . A method for estimating the value of  $m$  is given in [Ainsworth and Senior (1997)]. For problems with singularity, the value of  $m$  will be low near singular regions. The  $hp$  adaptivity procedure automatically performs  $h$  refinement near a singularity and  $p$  refinement outside of the singular regions.

### 4.3 Computational Subdomain Level-2

Level-2 regions are characterized as those with significant microstructural non-uniformities in the form of high local stresses or strains that would occur e.g. near a crack tip or free edge. High gradients in macroscopic variables and loss of RVE periodicity are expected in those regions. Scale effects are important in these regions, resulting in mesh-dependence of pure macroscopic computations. Adaptivity is used to switch from level-1 to level-2 elements for performing extended microscopic analysis. The microscopic model in level-2 elements is required to encompass considerable portions of the microstructure with large number of heterogeneities as shown in Fig. 9. Level-2 elements are constructed by filling macro level-1 elements with the exact microstructure at that location. The region  $\Omega_{l_2}^k$  constituting the  $k$ -th level-2 element, is obtained as the intersection of the entire microstructural region  $\Omega^\varepsilon$  with the boundary of the  $k$ -th level-1 element  $\Omega_{l_1}^k$ , i.e.

$$\Omega_{l_2}^k = \Omega^\varepsilon \cap \Omega_{l_1}^k \quad (14)$$

Steps in creating a level-2 element are itemized below

- Use adaptation criteria described in Section 6.2, to determine if a level-1 element needs to switch to level-2 element.
- Identify a region  $\Omega_{\hat{k}} \in \Omega^\varepsilon$  that is located in the same region in  $\Omega_{l_2}^k$  and that extends beyond  $\Omega_{l_2}^k$  by approximately two fiber lengths.

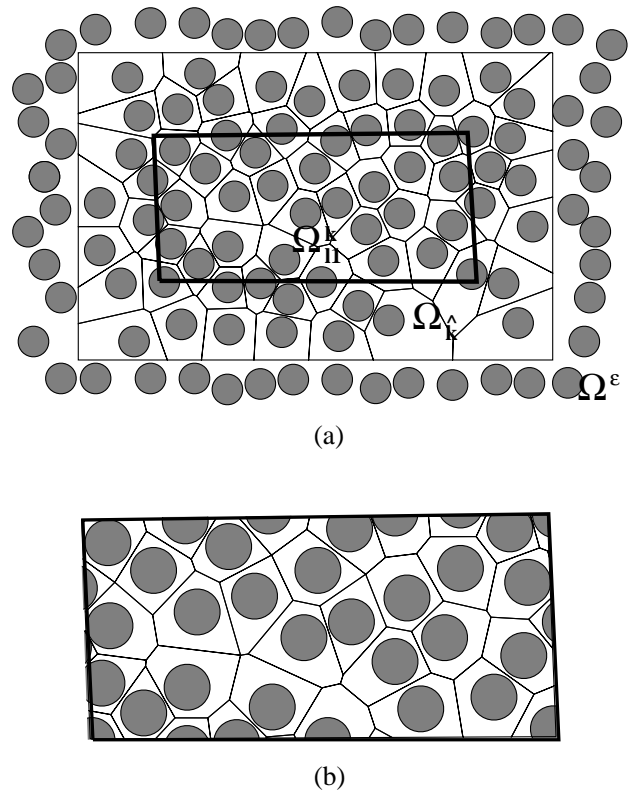


**Figure 9 :** (a) Level-1 element boundary superposed over the actual microstructure (b) Level-2 element formed by carving out the microstructure

- Tessellate the region  $\Omega_{\hat{k}}$  to generate a mesh of Voronoi cell elements as shown in Fig. 9(a).
- Carve out the region  $\Omega_{l_2}^k$  by superposing the boundary of  $\Omega_{l_1}^k$  on  $\Omega_{\hat{k}}$ . This procedure will result in dissecting some of the fibers on the boundary of  $\Omega_{l_2}^k$ . When this happens, additional nodes are generated on the Voronoi cell boundary at locations where the fiber surface and Voronoi cell edges intersects the boundary of  $\Omega_{l_2}^k$ . The dissected pieces of a fiber belong to two contiguous level-2 elements are joined together when the two contiguous elements share a common edge.

The high resolution model for level-2 elements with many heterogeneities entails prohibitively large computations with conventional finite element models. Consequently, the microstructure based Voronoi Cell Finite Element Model (VCFEM), which has been developed by the authors [Moorthy and Ghosh (1996, 1998, 2000)] in

modeling non-uniform heterogeneous materials is used for analyzing the level-2 elements. Extensive microstructural regions, obtained from micrographs, are efficiently modeled by this approach. In VCFEM, the computational mesh consists of multi-sided Voronoi polygons that naturally evolve by tessellation of the microstructure [Ghosh and Mukhopadhyay (1991)]. Each element in VCFEM consists of a heterogeneity (inclusion or void) with its immediate surrounding matrix. Accuracy of analysis is maintained for these relatively large multiphase elements by incorporating observed behavior of stress fields from micromechanics in an assumed stress hybrid finite element formulation [Moorthy and Ghosh (1996, 1998)]. This method has shown considerable success in modeling elastic-plastic problems [Moorthy and Ghosh (1996)] and problems with damage by particle cracking and debonding [Moorthy and Ghosh (1998); Ghosh, Ling, Majumdar and Kim (2000)]. VCFEM has been successful in significantly reducing computational degrees of freedom and current VCFEM computing effort is estimated to be  $\sim 60$ -70 times lower than most commercial FEM packages for modeling complex microstructures.

#### 4.3.1 Transition Elements between Level-0/1 and Level-2 Elements

The interface between the macroscopic displacement based level-0 or level-1 elements, and level-2 elements requires a layer of transition elements for creating a smooth transition of variables as shown in Fig. 8. These elements (*tr*) are essentially level-2 elements with a displacement constraint imposed at the interface with level-0/1 elements. In [Ghosh, Lee and Raghavan (2001)], a direct constraint has been imposed on Voronoi cell FEM nodes in the transition elements to conform with the displacement interpolation of the adjacent level-0/level-1 element boundaries.

Such a direct constraining process may however lead to local singularities in the transition element due to induced displacement discontinuities at the interface. To avert these spurious singularities, a special interfacial layer is introduced between the transition elements and the level-0/level-1 elements. As shown in Fig. 10, the left side corresponds to level-0/level-1 elements with lower order displacement polynomials on the boundary. The right side corresponds to the boundary of transition elements which consists of multiple edges, of Voronoi cell

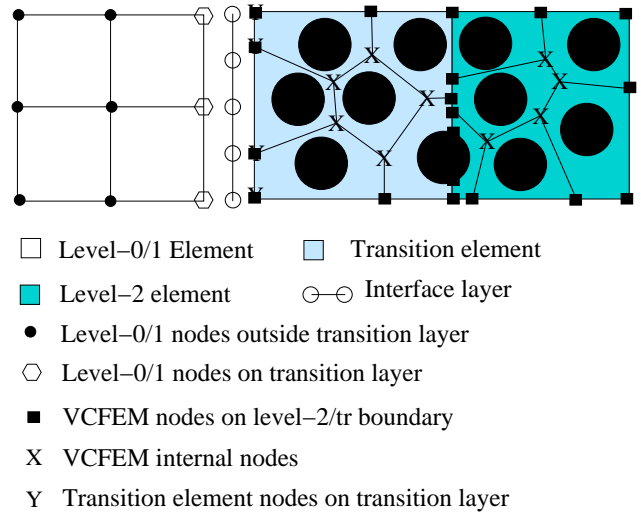


**Figure 10** : Interface constraint at the level-0/1 element and transition element

elements depending on the number of fibers. The intermediate boundary segment is generally chosen to have higher order interpolation than the adjacent level-0/level-1 element boundaries. As suggested in [Aminpour, Ransom and McCleary (1995)], Lagrange multipliers are used to satisfy the interfacial displacement continuity constraint in a weak sense. Comprehensively speaking, the total potential energy of the multi-level element mesh may be expressed as

$$\begin{aligned} \Pi = & \Pi_{\Omega_{l_0}} + \Pi_{\Omega_{l_1}} + \Pi_{\Omega_{l_2}} + \Pi_{\Omega_{tr}} \\ & + \int_{\Gamma_{int}} \lambda_i^{l_0/l_1} (v_i - u_i^{l_0/l_1}) d\Gamma \\ & + \int_{\Gamma_{int}} \lambda_i^{tr} (v_i - u_i^{tr}) d\Gamma \end{aligned} \quad (15)$$

where  $\Pi_{\Omega_{l_0}}$ ,  $\Pi_{\Omega_{l_1}}$ ,  $\Pi_{\Omega_{l_2}}$  and  $\Pi_{\Omega_{tr}}$  are the total potential energies for elements in level-0, level-1, level-2 subdomains and transition regions respectively.  $\Gamma_{int}$  corresponds to the interfacial layer.  $\lambda^{l_0/l_1}$  and  $\lambda^{tr}$  are Lagrange multipliers on  $\Gamma_{int}$ , corresponding to boundaries of  $\Omega_{l_0/l_1}$  and  $\Omega_{tr}$  respectively. The interfacial displacements on the boundaries of  $\Omega_{l_0/l_1}$  and  $\Omega_{tr}$  elements at the interface are designated as  $\mathbf{u}^{l_0/l_1}$  and  $\mathbf{u}^{tr}$ . The Euler's equations, obtained by the variation of Eq. 15 with respect to  $\mathbf{v}$ ,  $\lambda^{l_0/l_1}$  and  $\lambda^{tr}$ , are

$$\begin{aligned} \lambda_i^{l_0/l_1} = & (\sigma_{ij} n_j)^{l_0/l_1} = -\lambda_i^{tr} = -(\sigma_{ij} n_j)^{tr} \quad \text{and} \\ u_i^{l_0/l_1} = & u_i^{tr} = v_i \end{aligned} \quad (16)$$

where  $n_i$  is the unit outward normal vector, and  $\lambda_i^{10/11}$  and  $\lambda_i^{tr}$  correspond to the interface tractions on the boundaries of  $\Omega_{10/11}$  and  $\Omega_{tr}$  respectively.

## 5 Coupling of all Levels

The global stiffness matrix and load vectors are derived for the complete multi-scale model consisting of level-0, level-1, level-2 and transition elements. The computational domain ( $\Omega$ ) can be described as

$$\Omega = \{\Omega_{10} \cup \Omega_{11} \cup \Omega_{12} \cup \Omega_{tr}\} \quad (17)$$

- $\Omega_{10} = \bigcup_{k=1}^{N_{10}} E_{10}$  - Domain comprised of  $N_{10}$  level-0 elements with boundary  $\partial\Omega_{10}$
- $\Omega_{11} = \bigcup_{k=1}^{N_{11}} E_{11}$  - Domain comprised of  $N_{11}$  level-1 elements with boundary  $\partial\Omega_{11}$
- $\Omega_{12} = \bigcup_{k=1}^{N_{12}} E_{12}$  - Domain comprised of  $N_{12}$  level-2 elements with boundary  $\partial\Omega_{12}$
- $\Omega_{tr} = \bigcup_{k=1}^{N_{tr}} E_{tr}$  - Domain comprised of  $N_{tr}$  transition elements with boundary  $\partial\Omega_{tr}$

The boundary of the complete domain  $\Gamma$  can be written as

$$\Gamma = \{\Gamma_{10} \cup \Gamma_{11} \cup \Gamma_{12} \cup \Gamma_{tr}\} \quad (18)$$

where,  $\Gamma_{10}$ ,  $\Gamma_{11}$ ,  $\Gamma_{12}$ ,  $\Gamma_{tr}$  are defined as  $\Gamma_{10} = \partial\Omega_{10} \cap \Gamma$ ,  $\Gamma_{11} = \partial\Omega_{11} \cap \Gamma$ ,  $\Gamma_{12} = \partial\Omega_{12} \cap \Gamma$ ,  $\Gamma_{tr} = \partial\Omega_{tr} \cap \Gamma$  respectively. The equation for the principle of virtual work

for the entire domain can be expressed as

$$\begin{aligned} & \int_{\Omega_{10}} \Sigma_{ij} \frac{\partial \delta u_i^{10}}{\partial x_j} d\Omega - \int_{\Omega_{10}} f_i \delta u_i^{10} d\Omega \\ & + \int_{\Omega_{11}} \Sigma_{ij} \frac{\partial \delta u_i^{11}}{\partial x_j} d\Omega - \int_{\Omega_{11}} f_i \delta u_i^{11} d\Omega \\ & + \int_{\Omega_{12}} \sigma_{ij} \frac{\partial \delta u_i^{12}}{\partial x_j} d\Omega - \int_{\Omega_{12}} f_i \delta u_i^{12} d\Omega \\ & + \int_{\Omega_{tr}} \sigma_{ij} \frac{\partial \delta u_i^{tr}}{\partial x_j} d\Omega - \int_{\Omega_{tr}} f_i \delta u_i^{tr} d\Omega \\ & - \int_{\Gamma_{10}} t_i \delta u_i^{10} d\Gamma - \int_{\Gamma_{11}} t_i \delta u_i^{11} d\Gamma \\ & - \int_{\Gamma_{12}} t_i \delta u_i^{12} d\Gamma - \int_{\Gamma_{tr}} t_i \delta u_i^{tr} d\Gamma \\ & + \delta \int_{\Gamma_{int}} \lambda_i^{10/11} (v_i - u_i^{10/11}) d\Gamma + \delta \int_{\Gamma_{int}} \lambda_i^{tr} (v_i - u_i^{tr}) d\Gamma = 0 \end{aligned} \quad (19)$$

An implicit assumption is made in this equation that the traction continuity between level-0 and level-1, and level-2 and transition elements, are satisfied in a weak sense.

The terms in the box of Eq. 19 for  $\Omega_{12}$  and  $\Omega_{tr}$  are analyzed using the Voronoi cell finite element method and should be integrated with the other terms obtained by conventional displacement based finite element analysis.

The VCFEM employs the assumed stress hybrid formulation with independent assumptions on equilibrated stress fields ( $\boldsymbol{\sigma}$ ) in the matrix ( $\Omega_m$ ) and fiber phases ( $\Omega_c$ ) of each element, and compatible displacement fields  $\mathbf{u}^e$  on the element boundary  $\partial\Omega_e$  and  $\mathbf{u}^c$  on the matrix-inclusion interface  $\partial\Omega_c$  as shown in Fig. 11. The element complimentary energy functional is given by

$$\begin{aligned} \Pi_e^C(\boldsymbol{\sigma}, \mathbf{u}^e, \mathbf{u}^c) &= \int_{\Omega_e} \boldsymbol{\sigma} : \mathbf{S} : \boldsymbol{\sigma} d\Omega - \int_{\partial\Omega_e} \boldsymbol{\sigma} \cdot \mathbf{n}^e \cdot \mathbf{u}^e d\partial\Omega \\ &+ \int_{\Gamma_{tm}} \bar{\mathbf{t}} \cdot \mathbf{u}^e d\Gamma + \int_{\partial\Omega_c} (\boldsymbol{\sigma}^m - \boldsymbol{\sigma}^c) \cdot \mathbf{n}^c \cdot \mathbf{u}^c d\partial\Omega \end{aligned} \quad (20)$$

where  $\mathbf{S}$  is the elastic compliance tensor,  $\mathbf{n}^e$  and  $\mathbf{n}^c$  are the outward normals on  $\partial\Omega_e$  and  $\partial\Omega_c$  respectively and  $\bar{\mathbf{t}}$  is the prescribed traction on the boundary  $\Gamma_{tm}$ . The total energy functional for a level-2 element containing  $N_{vc}$  Voronoi

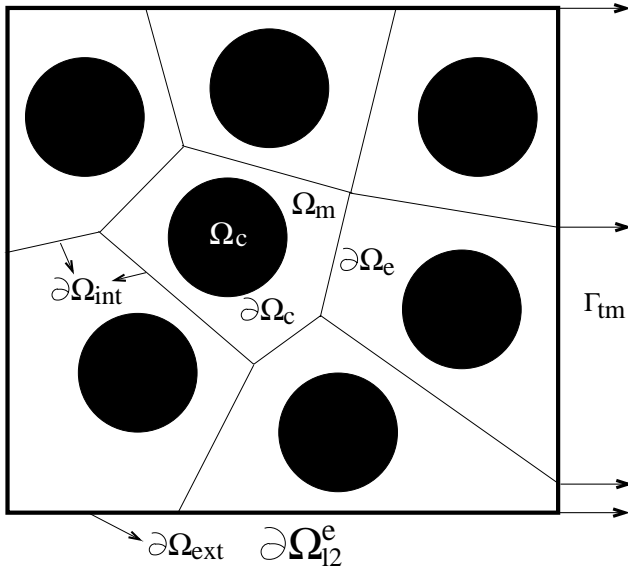


**Figure 11** : A Level-2 element with Voronoi cell finite elements

cell elements can be written as

$$\begin{aligned} \Pi^C &= \sum_{e=1}^{N_{vc}} \Pi_e^C = \sum_{e=1}^{N_{vc}} \int_{\Omega_e} \boldsymbol{\sigma} : \mathbf{S} : \boldsymbol{\sigma} d\Omega \\ &\quad - \sum_{e=1}^{N_{vc}} \int_{\partial\Omega_e} \boldsymbol{\sigma} \cdot \mathbf{n}^e \cdot \mathbf{u}^e d\partial\Omega + \sum_{e=1}^{N_{vc}} \int_{\Gamma_{tm}} \bar{\mathbf{t}} \cdot \mathbf{u}^e d\Gamma \\ &\quad + \sum_{e=1}^{N_{vc}} \int_{\partial\Omega_c} (\boldsymbol{\sigma}^m - \boldsymbol{\sigma}^c) \cdot \mathbf{n}^c \cdot \mathbf{u}^c d\partial\Omega \end{aligned} \quad (21)$$

The variation of the above equation with respect to the element boundary displacements  $\mathbf{u}^e$  results in

$$\delta\Pi^C = - \sum_{e=1}^{N_{vc}} \int_{\partial\Omega_e} \boldsymbol{\sigma} \cdot \mathbf{n}^e \cdot \delta\mathbf{u}^e d\partial\Omega + \sum_{e=1}^{N_{vc}} \int_{\Gamma_{tm}} \bar{\mathbf{t}} \cdot \delta\mathbf{u}^e d\Gamma \quad (22)$$

The boundaries of all Voronoi cells can be split as

$$\sum_{e=1}^{N_{vc}} \partial\Omega_e = \partial\Omega^{int} \cup \partial\Omega^{ext} \quad (23)$$

where  $\partial\Omega^{ext}$  corresponds to external Voronoi cell element boundaries that coincide with level-2/transition element boundary and  $\partial\Omega^{int}$  corresponds to all the other internal boundaries of Voronoi cell elements. The external element boundaries  $\partial\Omega^{ext}$  are identified by thick lines in

Fig. 11. Eq. 22 can be re-written as

$$\begin{aligned} \delta\Pi^C &= - \sum_{e=1}^{N_{vc}} \int_{\partial\Omega^{int}} \boldsymbol{\sigma} \cdot \mathbf{n}^e \cdot \delta\mathbf{u}^e d\partial\Omega - \\ &\quad \sum_{e=1}^{N_{vc}} \int_{\partial\Omega^{ext}} \boldsymbol{\sigma} \cdot \mathbf{n}^e \cdot \delta\mathbf{u}^e d\partial\Omega + \sum_{e=1}^{N_{vc}} \int_{\Gamma_{tm}} \bar{\mathbf{t}} \cdot \delta\mathbf{u}^e d\Gamma \end{aligned} \quad (24)$$

In the virtual work equation Eq. 19, the boxed terms corresponding to energy in level-2 and transition elements can be re-written using divergence theorem, in the absence of body forces as

$$\int_{\Omega_{l2/tr}^e} \boldsymbol{\sigma} \cdot \nabla \mathbf{u}^e d\Omega = \int_{\partial\Omega_{l2/tr}^e} \boldsymbol{\sigma} \mathbf{n}^e \cdot \delta\mathbf{u}^e d\Gamma - \int_{\Omega_{l2/tr}^e} \nabla \boldsymbol{\sigma} \cdot \mathbf{u}^e d\Omega \quad (25)$$

The first term in Eq. 25 is obtained as the contribution to the stiffness from all Voronoi cells and can be calculated using Eq. 24 as

$$\begin{aligned} \int_{\partial\Omega_{l2/tr}^e} \boldsymbol{\sigma} \cdot \mathbf{n}^e \cdot \delta\mathbf{u}^e d\Gamma &= - \sum_{e=1}^{N_{vc}} \int_{\partial\Omega_e^{vc}} \boldsymbol{\sigma} \cdot \mathbf{n}^e \cdot \delta\mathbf{u}^e d\partial\Omega \\ &\quad + \int_{\Gamma_{tm}} \bar{\mathbf{t}} \cdot \delta\mathbf{u}^e d\Gamma + \int_{\partial\Omega^{int}} \boldsymbol{\sigma} \cdot \mathbf{n}^e \cdot \delta\mathbf{u}^e d\partial\Omega \end{aligned} \quad (26)$$

The last term in Eq. 25 drops out since the analysis is performed using VCFEM, which uses an equilibrated stress field. The contribution to the stiffness matrix from level-2 elements may therefore be calculated by assembling the stiffness contributions from all VCFEM elements using Eq. 22 and condensing out the internal degrees of freedom on  $\partial\Omega^{int}$ . To achieve this, the displacement field along the edges of VCFEM elements are interpolated by

$$\{\mathbf{u}^e\} = [L_{vc}]\{U_{vc}\} \quad (27)$$

The degrees of freedom  $U_{vc}$  can be separated into  $U_{l2}^{ext}$  and  $U_{l2}^{int}$  depending on whether they belong to  $\partial\Omega^{ext}$  or  $\partial\Omega^{int}$  respectively. The stiffness matrix and the load vector of the ensemble of all Voronoi cell elements belonging to a level-2 element can be partitioned as

$$\begin{bmatrix} K_{l2}^{ext,ext} & K_{l2}^{ext,int} \\ K_{l2}^{int,ext} & K_{l2}^{int,int} \end{bmatrix} \begin{Bmatrix} U_{l2}^{ext} \\ U_{l2}^{int} \end{Bmatrix} = \begin{Bmatrix} F_{l2}^{ext} \\ F_{l2}^{int} \end{Bmatrix} \quad (28)$$

Static condensation of the internal degrees of freedom leads to

$$\begin{aligned} &\left[ [K_{l2}^{ext,ext}] - [K_{l2}^{ext,int}] [K_{l2}^{int,int}]^{-1} [K_{l2}^{int,ext}] \right] \{U_{l2}^{ext}\} \\ &= \{F_{l2}^{ext}\} - [K_{l2}^{ext,int}] [K_{l2}^{int,int}]^{-1} \{F_{l2}^{int}\} \end{aligned} \quad (29)$$

The above equation is then used in global assembly.

The displacements  $u_i^{I0}$  and  $u_i^{I1}$  in level-0 and level-1 elements are interpolated by the standard or hierarchical shape functions based on Legendre polynomials as [Ainsworth and Senior (1997)]

$$\{u\}^{I0/I1} = [N_{I0/I1}]\{U_{I0/I1}\} = [N_{I0/I1}^I N_{I0/I1}^O]\left\{ \begin{array}{c} U_{I0/I1}^I \\ U_{I0/I1}^O \end{array} \right\} \quad (30)$$

where  $U_{I0/I1}^I$  corresponds to the nodal degrees of freedom at the interface with transition elements and  $U_{I0/I1}^O$  are all others. A similar separation can also done for transition elements into displacements on this interface,  $U_{tr}^I$  and otherwise,  $U_{I2/tr}^O$ .

The displacements and the Lagrange multipliers on the intermediate boundary segment are interpolated from nodal values using suitably assumed shape functions as

$$\{v\} = [L_{int}]\{U_{int}\}, \quad \{\lambda^{I0/I1}\} = [L_{\lambda^{I0/I1}}]\{\Lambda_{I0/I1}\} \\ \{\lambda^{tr}\} = [L_{\lambda^{tr}}]\{\Lambda_{tr}\} \quad (31)$$

Substituting interpolations from Eq. 29, Eq. 30 and Eq. 31 in Eq. 19 results in a coupled set of matrix equations for the multi-level domain. The global assembly leads to the following coupled set of equations

$$\begin{bmatrix} K_{I0/I1}^{I,I} & K_{I0/I1}^{I,O} & 0 & 0 & 0 & P_{I0/I1} & 0 \\ K_{I0/I1}^{O,I} & K_{I0/I1}^{O,O} & 0 & 0 & 0 & 0 & 0 \\ 0 & 0 & K_{tr}^{I,I} & K_{I2/tr}^{I,O} & 0 & 0 & P_{tr} \\ 0 & 0 & K_{I2/tr}^{O,I} & K_{I2/tr}^{O,O} & 0 & 0 & 0 \\ 0 & 0 & 0 & 0 & 0 & Q_{I0/I1} & Q_{tr} \\ P_{I0/I1}^T & 0 & 0 & 0 & Q_{I0/I1}^T & 0 & 0 \\ 0 & 0 & P_{tr}^T & 0 & Q_{tr}^T & 0 & 0 \end{bmatrix} \begin{Bmatrix} U_{I0/I1}^I \\ U_{I0/I1}^O \\ U_{tr}^I \\ U_{I2/tr}^O \\ U_{int} \\ \Lambda_{I0/I1} \\ \Lambda_{tr} \end{Bmatrix} = \begin{Bmatrix} F_{I0/I1}^I \\ F_{I0/I1}^O \\ F_{tr}^I \\ F_{I2/tr}^O \\ 0 \\ 0 \\ 0 \end{Bmatrix} \quad (32)$$

The notation corresponding to the superscript  $I$  represents quantities on the interface whereas those with the superscript  $O$  are on the regions other than interface. The

submatrices  $K_{I0/I1}$ ,  $K_{I2}$  and  $K_{tr}$  and the vectors  $F_{I0/I1}$ ,  $F_{I2}$  and  $F_{tr}$  correspond to stiffness matrices and load vectors from the respective subdomains given as

$$[K_{I0/I1}] = \int_{\Omega_{I0/I1}} [B]^T [E] [B] d\Omega \\ \{F_{I0/I1}\} = \int_{\Omega_{I0/I1}} [N_{I0/I1}]^T \{f\} d\Omega + \int_{\Gamma_{I0/I1}} [N_{I0/I1}]^T \{t\} d\Gamma \quad (33)$$

where  $[B]$  is the strain-displacement matrix. The stiffness  $[K_{I2/tr}]$  and the load vectors  $\{F_{I2/tr}\}$  for level-2 and transition elements are obtained by solving VCFEM using the procedure described in [Moorthy and Ghosh (1996)]. The coupling between the level-0/1 and transition elements is achieved through the  $[P]$  and  $[Q]$  matrices, which are

$$[P_{I0/I1}] = - \int_{\Gamma_{int}} [N_{I0/I1}]^T [L_{\lambda^{I0/I1}}] d\Gamma \\ [P_{tr}] = - \int_{\Gamma_{int}} [L_{tr}]^T [L_{\lambda^{tr}}] d\Gamma \\ [Q_{I0/I1}] = \int_{\Gamma_{int}} [L_{int}]^T [L_{\lambda^{I0/I1}}] d\Gamma \\ [Q_{tr}] = \int_{\Gamma_{int}} [L_{int}]^T [L_{\lambda^{tr}}] d\Gamma \quad (34)$$

The system of equations is solved using an iterative solver with Lanczos method.

## 6 Discretization and Modeling Error Indicators

The errors associated with the multi-level model are classified into two groups, viz., discretization errors and modeling errors.

### 6.1 Discretization Error

Discretization error in level-0/1 elements is a result of insufficient orders of interpolation in the finite element model. The  $hp$ - adaptive mesh refinement suggested in [Ainsworth and Senior (1997)] is adopted in this paper to reduce the discretization error. The steps involved in this process are as follows

- Evaluate the energy norm of the local error  $\phi_k$  for element  $k$ , by solving the residual in the principal of virtual work as

$$\int_{\Omega_{I0/I1}^k} \Sigma_{ij}(\Phi_k) e_{ij}(\mathbf{v}) d\Omega = \int_{\Omega_{I0/I1}^k} f_i v_i d\Omega \\ - \int_{\Omega_{I0/I1}^k} \Sigma_{ij}(\mathbf{u}_{I0/I1}) e_{ij}(\mathbf{v}) d\Omega + \int_{\Gamma^k} (g_k)_i v_i d\Gamma \quad (35)$$

where  $(g_k)_i$  is the traction discontinuity on the element boundary  $\Gamma^k$ .

- Identify elements for  $hp$ - adaptivity from the condition  $\phi_k \geq C_1(\phi_k)_{\max}$ , where  $(\phi_k)_{\max}$  is the maximum elemental local error. If an element is a candidate for adaptation, an exponent  $m$  is evaluated to determine the type of adaptivity i.e if  $p + 2 \leq m$

- then  $p$  refinement
- else  $h$  refinement

is performed. The singularity indicator  $m$  can be obtained by solving

$$\|\phi\|_k^2 = \|\phi_{p+q}\|_k^2 + C_k^2(p+q)^{-2(m-1)} \quad (36)$$

for three different values of  $q$  as outlined in [Ainsworth and Senior (1997)].

## 6.2 Modeling Error

### Transition from level-0 to level-1 :

Modeling errors for level-0 and level-1 elements evolve at regions where macroscopic uniformity and microscopic periodicity become invalid. Various conditions, depending on the physics of the problem being are proposed. Two examples of such criteria considered in this paper are given below.

1. If a macroscopic stress  $\Sigma_{ij}$  is important, criteria based on the gradients of this stress can be proposed. Transition from level-0 to level-1 for an element  $k$  is performed if

$$E_k \geq C_2 E_{avg} \quad (37)$$

where  $E_{avg} = (\frac{\sum_{k=1}^{NE} E_k^2}{NE})^{1/2}$  and  $E_k^2 = \frac{\int_{\Gamma^k} [|\Sigma_{ij}|]^2 d\Gamma}{\int_{\Gamma^k} d\Gamma}$ .  $NE$  is the total number of elements and  $[[ \ ]]$  is the jump operator.

2. When traction gradient is critical [Raghavan, Moorthy, Ghosh and Pagano (2001)], level-0 to level-1 transition for element  $k$  will be made if

$$E_k \geq C_3 E_{avg} \quad (38)$$

where  $E_{avg} = (\frac{\sum_{k=1}^{NE} E_k^2}{NE})^{1/2}$  and

$E_k^2 = \frac{\int_{\Gamma^k} (|[T_x]|^2 + |[T_y]|^2) d\Gamma}{\int_{\Gamma^k} d\Gamma}$  and  $T_x$  and  $T_y$  are tractions in  $x$  and  $y$  directions respectively.

### Transition from level-1 to level-2 :

Criteria for transition from level-1 to level-2, is based on observation of variables in the RVE and prediction of departure from periodicity. In this work, large local stresses in the matrix/fiber or interfaces are assumed to indicate such departures. Two alternative criteria are used in this paper.

1. Level-1 to level-2 transition takes place if the local microscopic equivalent stress  $\sigma_{eqv} = \sqrt{\frac{3}{2}\sigma'_{ij}\sigma'_{ij}}$  exceeds the average. The equivalent stress is a good indicator for damage, especially in plasticity dominated problems. Level-1 to level-2 transition is made if

$$\begin{aligned} (\sigma_{eqv}^m)_{\max} &\geq C_4 (\sigma_{eqv}^m)_{\text{avg}} \quad \text{or} \\ (\sigma_{eqv}^c)_{\max} &\geq C_4 (\sigma_{eqv}^c)_{\text{avg}} \end{aligned} \quad (39)$$

at more than 1% of all integration points in the RVE.  $(\sigma_{eqv}^m)_{\max}$  and  $(\sigma_{eqv}^m)_{\text{avg}}$ , and  $(\sigma_{eqv}^c)_{\max}$  and  $(\sigma_{eqv}^c)_{\text{avg}}$  represent the maximum and average equivalent stresses in the matrix and in the fiber.

2. Transition from level-1 to level-2 takes place if

$$|T| \geq C_5 |T_{avg}| \quad (40)$$

where  $T$  represents the local interfacial traction ( $\sqrt{T_n^2 + T_t^2}$ ) evaluated on the fiber/matrix interface.  $T_{avg}$  is the average traction on the fiber/matrix boundary and is given by  $\frac{\sum_{i=1}^{NI} T}{NI}$ , where  $NI$  is the total number of integration points on the fiber/matrix interface in the RVE. Since debonding is an important failure mechanism in fiber reinforced composites, this criteria is expected to warrant significant amount of debonding in the microstructure.

All constants  $C_1$  to  $C_5$  are chosen from trial numerical experiments.

## 7 Numerical Examples - Composite Plate with a Hole

Numerical experiments are conducted to demonstrate the effectiveness of the multi-scale model. Two examples, one of a composite plate and another of a composite laminate are considered.

### 7.1 Composite Plate with a Hole

A fiber reinforced composite plate with a hole as shown in Fig. 1 is analyzed. The dimensions of the composite plate are  $W = 22.86 \text{ mm}$ ,  $L = 114.285 \text{ mm}$  and  $r = 6.858 \text{ mm}$ . The representative microstructure of the plate at the point A is shown in Fig. 1 with dimensions  $100 \mu\text{m} \times 79.09 \mu\text{m}$ . All fibers are assumed to possess the same radius value of  $1.75 \mu\text{m}$ . Average fiber spacing is around  $3.4 \mu\text{m}$ . The estimated total number of fibers for this quarter plate is approximately 8 million. The matrix material is epoxy with properties  $E_m = 3.8 \text{ GPa}$  and  $\nu_m = 0.34$ . The graphite fiber properties are  $E_f = 380.0 \text{ GPa}$  and  $\nu_f = 0.20$ . The plate is subjected to a load of unity along the  $y$  direction on the top face. A statistically equivalent RVE for this plate is evaluated as described in Section 3 and is found to contain 18 fibers.

The effective modulus (in GPa) calculated by homogenization for this SERVE is given by  $E_{1111} = 10.51$ ,  $E_{1122} = 4.49$ ,  $E_{1133} = 4.23$ ,  $E_{2222} = 11.19$ ,  $E_{1212} = 2.85$ ,  $E_{3333} = 127.35$ . Using this modulus the macroscopic model is constructed with 300 level-0 elements. Generally no singularities are expected in the solution of the problem. Consequently, discretization error would result in  $p$ -adaptivity being predominant. While a  $p$ -adaptation would suffice for the problem, the  $h$ -refinement facilitates for significantly smaller regions of localized modeling error identification and hence realization of fewer elements making level transitions. The  $h$ -adaptations are executed to a minimum macroscopic element size of  $25 \mu\text{m}$  and no more. Level-0 to level-1 transition takes place according to Eq. 37 as specified in Section 6.2 with the value of  $C_2$  taken to be 1.5. Level-1 to level-2 transition takes place according to Eq. 39 as specified in Section 6.2 with the value of  $C_4$  taken to be 4.0. The adapted multi-scale mesh, shown in Fig. 12, consists of 1091 level-0 elements, 2 level-1 elements, 3 transition elements and 2 level-2 elements. The mesh in the critical region is circled and shown in Fig. 12(b). The microstructure for the level-2 and transition elements is shown in Fig. 12(c). The macroscopic contour plot of  $\Sigma_{yy}$  stress and microscopic contour plot of  $\sigma_{yy}$  stress for the element close to the critical region A is shown in Fig. 13. It can be seen that the maximum microscopic stresses are at least one order higher than the macroscopic values. The maximum microscopic stresses is near the point where two or more fibers are located close to each other.

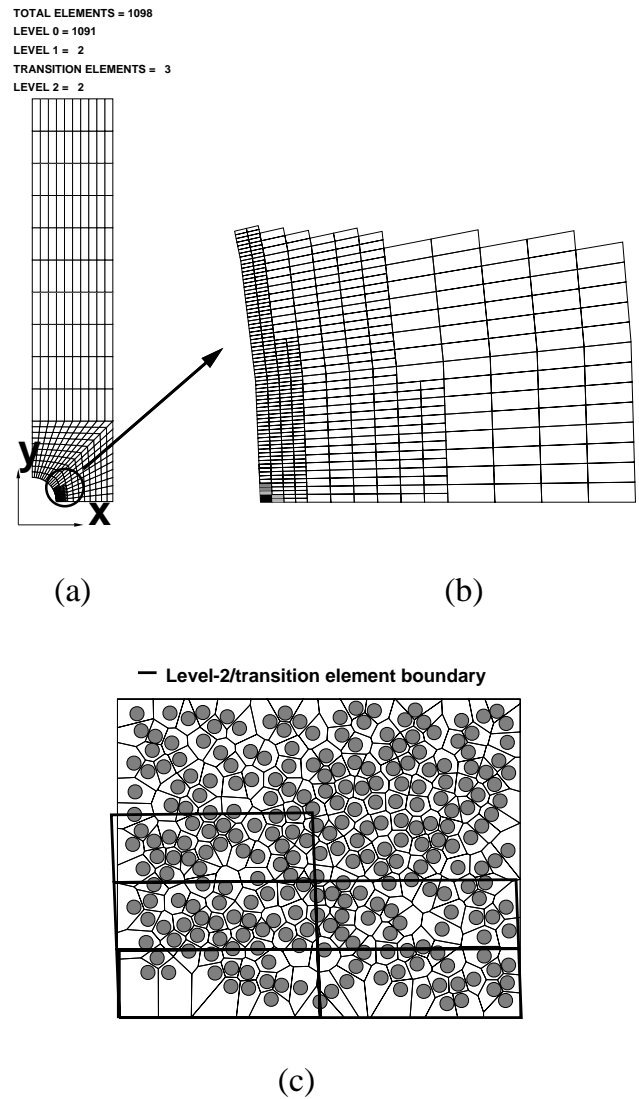


**Figure 12 :** (a)  $h$  adapted multi-level mesh (b) Mesh around local circled area (c) Microstructure of level-2/transition elements

### 7.2 Free Edge Composite Laminate Subjected to Extensional Loading

The performance of the multi-scale model in the presence of singularity is demonstrated with this example. The composite laminate consists of randomly distributed fibers on the top and bottom whereas the middle portions consists only of matrix material. With effective modulus theory this architecture corresponds to a homogenized

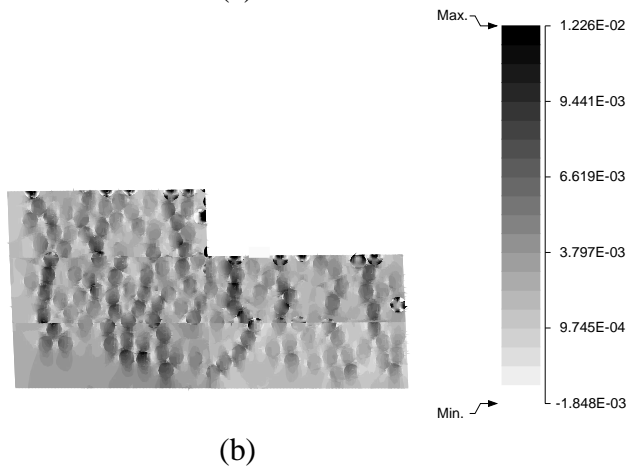
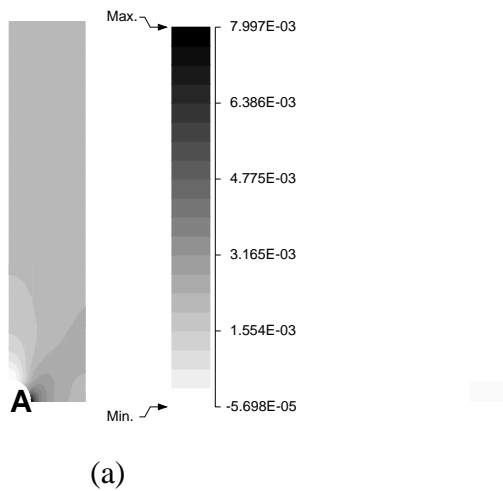


**Figure 13 :** (a) Contour plot of macroscopic  $\Sigma_{yy}$  stress for the plate with a hole (b) Contour plot of microscopic  $\sigma_{yy}$  stress for the macroscopic element close to point A

material sandwiched between two composite plies. The laminate is subjected to extensional out-of-plane loading along the fiber direction as shown in Fig. 14(a).

The microstructure of the laminate around the free edge point A is assumed to be same as in the previous problem. The dimension of the cross section is  $64\text{ mm} \times 32\text{ mm}$ . The out-of-plane loading, is simulated using a generalized plane strain condition with prescribed  $\epsilon_{zz} = 1$ . The distribution of the microstructure is assumed to symmetric about the  $x$  and  $y$  axes. Due to symmetry in the  $xz$  and  $yz$  planes only one quarter of the laminate is modeled. Symmetric boundary conditions are employed on the surfaces  $x = 0$  and  $y = 0$ , and the top and right surfaces are assumed to be traction free. The top portion

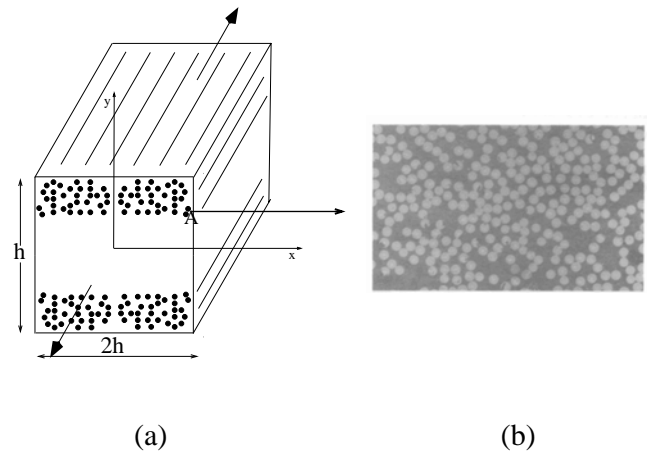


**Figure 14 :** (a) Composite laminate subjected to extensional loading (b) Optical micrograph of the microstructure near point A

of the laminate is modeled with effective properties obtained by homogenization. The initial mesh in the multi-level model consists of 200 level-0 4-noded bilinear or QUAD4 elements. The discretization error in the homogenized model is reduced by performing  $hp$ -adaptations. The presence of free edge at the composite-monolithic material interface causes a singularity in  $\sigma_{yy}$  stress. Due to the singularity,  $h$  adaptivity is dominant near the free edge, while regions far away from the free edge are  $p$  adapted.

The  $hp$ -adapted mesh is shown in Fig. 15(a) with a blow-up of the mesh near the free edge is shown in Fig. 15 (b).

Due to the requirement of traction continuity at the material interface level-0 to level-1 transition is made according to Eq. 38. For the level-1 to level-2 transition the criteria in Eq. 40 is used. The parameter  $C_3$  and  $C_5$  are chosen to be 2.5 and 1.25 respectively. The evolved multi-level model consists of 513 level-0 elements, 7 level-1 elements, 3 transition elements and 1 level-2 element. The microstructure of the macroscopic element close to the free edge is shown in Fig. 15(c). The macroscopic  $\Sigma_{yy}$  stress singularity at the material interface  $y = \frac{h}{4}$  is shown in Fig. 16. The figure also shows microscopic  $\sigma_{yy}$  stress near the free edge obtained from the multi-scale solution. It can be observed stress singularity observed at the free edge in the effective modulus solution is not present in the multi-scale solution. The macroscopic contour plot

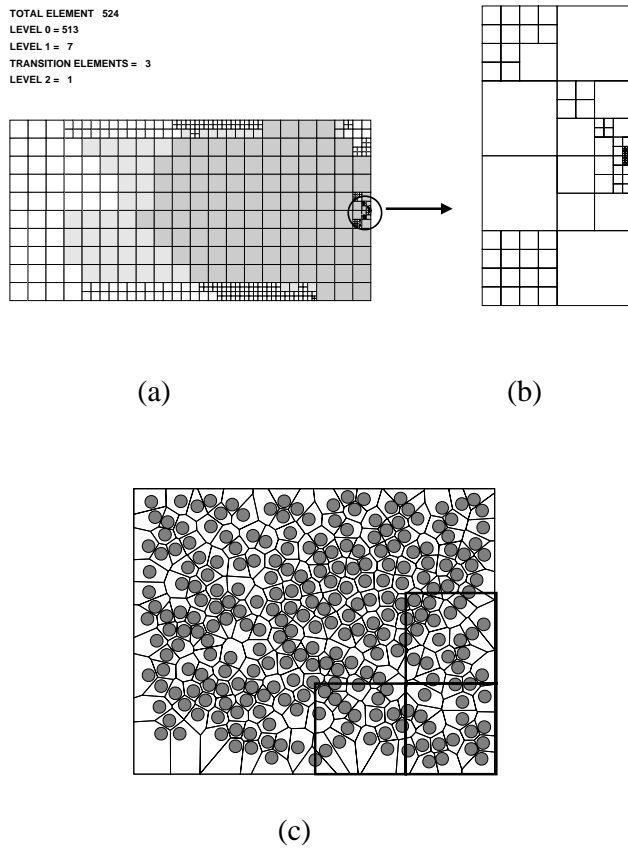


**Figure 15 :** (a)  $hp$ - adapted multi-level mesh (b) Mesh around local circled area (c) Microstructure of level-2/transition elements near the free edge

of  $\Sigma_{yy}$  stress is shown in Fig. 17. Fig. 17 also shows the distribution of microscopic  $\sigma_{yy}$  stress for the macroscopic element close to the free edge.

It can be noticed that the microscopic stress are atleast 2 orders higher than the macroscopic stress and occur in the fibers close to the free edge. The artificial interface created in the effective modulus solution is avoided in the multi-scale model thus providing with accurate stresses in critical regions.

### 8 Conclusion

This paper presents an adaptive multi-level computational model that combines a conventional displacement based finite element model with a microstructural Voronoi cell finite element model for multi-scale analysis of composite materials. The model is developed with the capability to analyze both macroscopic and micro-

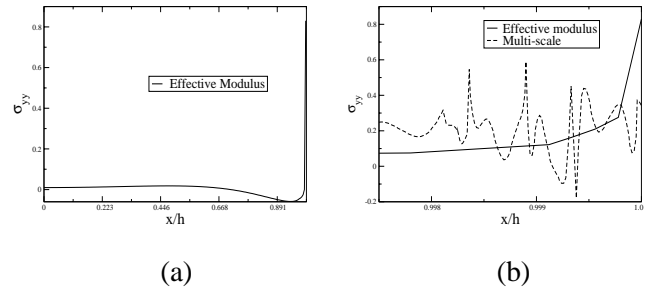


**Figure 16 :** (a) Macroscopic  $\Sigma_{yy}$  stress at  $y = \frac{h}{4}$  obtained with the homogenized model (b) Microscopic  $\sigma_{yy}$  stress at  $y = \frac{h}{4}$  near the free edge obtained with multi-scale model

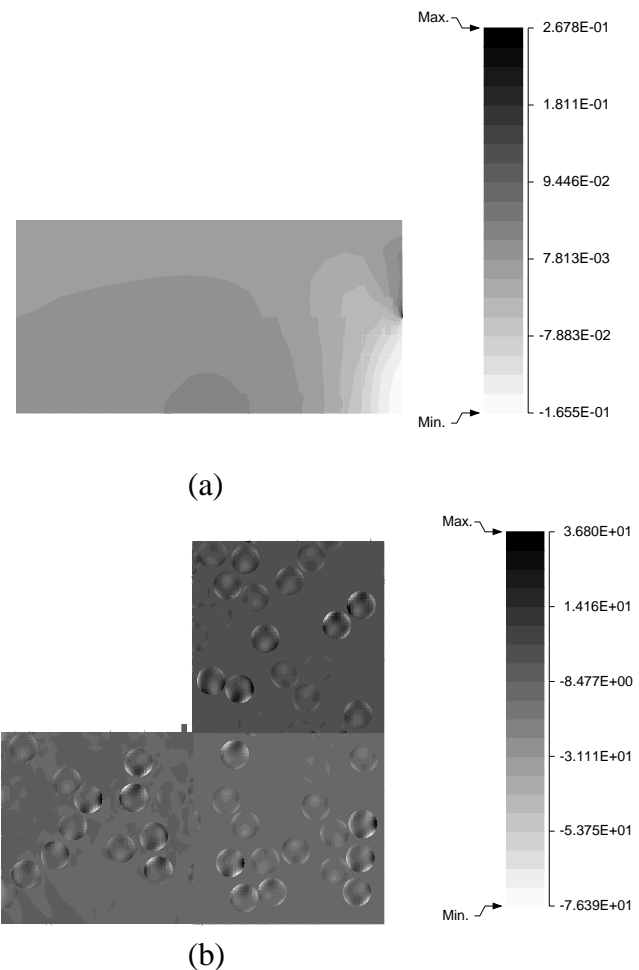


**Figure 17 :** (a) Contour plot of macroscopic  $\Sigma_{yy}$  stress for the composite laminate (b) Contour plot of microscopic  $\sigma_{yy}$  stress for the macroscopic element near the free edge

scopic stresses and strains in real composite structures with non-uniform microstructural heterogeneities as obtained from optical or scanning electron micrographs. Three levels of hierarchy, with different resolutions, are introduced in this model to overcome shortcomings posed by modeling and discretization errors. Among the three levels are: (a) level-0, where pure macroscopic analysis is conducted using effective properties obtained by homogenization of variables in a statistical equivalent RVE; (b) level-1, which are intermediate regions of macro-micro coupled modeling, used for signaling the switch over from macroscopic analyses to pure microscopic analyses; and (c) level-2 regions of pure microscopic modeling where critical events in the microstructure are expected to occur. The adaptive Voronoi cell finite element model is utilized effectively for analysis of extended microstructural regions with high efficiency and accuracy. Special transition elements between level-0/1 and level-2 elements provide the necessary constraint conditions to facilitate smooth transition from macroscopic to microscopic analysis.

Identification of statistically equivalent RVE (SERVE) for a non-uniform microstructure, is essential for evaluating the effective properties for use in level-0 and level-1 elements. The use of different correlation functions based on statistical principles offers a systematic way of identifying a bounded SERVE, which possess the similar effective properties as that of the entire local microstructural ensemble. Upon the determination of SERVE's for actual microstructures, microstructural analyses with homogenization is performed in this paper to demonstrate the convergence of effective properties as well as microscopic stresses as functions of the SERVE size.

Discretization error in the macroscopic computations of level-0 and level-1 elements is reduced by performing  $h$  and  $hp$  adaptations. Various modeling error criteria are experimented with, based on the physics of the problem considered. For the examples conducted, stress or traction gradients criteria are used for the level-0 to level-1 switch. High local microscopic stresses and interface tractions are used as modeling error criteria for making the transition from level-1 to level-2 elements. Two numerical examples of a composite plate with a hole, and a composite laminate comprised of a heterogeneous layer

and a monolithic layer, are solved to demonstrate the ability of the multi-scale computational model in analyzing complex heterogeneous structures. Extension of this to model to determine the initiation and propagation of failure due to fiber/matrix interfacial debonding is currently in progress.

**Acknowledgement:** This work has been supported by the Air Force Office of Scientific Research through grant No. F49620-98-1-01-93 (Program Director: Dr. B. L. Lee). This sponsorship is gratefully acknowledged. Computer support by the Ohio Supercomputer Center through grant # PAS813-2 is also gratefully acknowledged.

## References

- Ainsworth, M.; Senior, B.** (1997): Aspects of adaptive  $hp$ -finite element method: Adaptive strategy, conforming approximation and efficient solvers, *Comput. Meth. Appl. Mech. Engrg.*, vol. 150, pp. 65-87.
- Aminpour, M. A.; Ransom, J. B.; McCleary, S. L.** (1995): A coupled analysis method for structures with independently modeled finite element subdomains, *Int. Jour. Num. Meth. Engrg.*, vol. 38, pp. 3695-3718.
- Babuska, I.; Szabo, B.** (1991): *Finite Element Analysis*, John Wiley & Sons, Inc.
- Bensousan A.; Lions J.L.; Papanicoulau G.** (1978): Asymptotic analysis for periodic structures, *North Holland*, Amsterdam.
- Beran, M. J.** (1968): *Statistical Continuum Theories, Monographs in statistical physics*, vol. 9, Interscience Publishers New York-London-Sydney.
- Böhm, H.J.; Han, W.; Eckschlager, A.** (2004): Multi-inclusion unit cell studies of reinforcement stresses and particle failure in discontinuously reinforced ductile matrix composites, *CMES: Computer Modeling in Engineering & Sciences*, Vol. 5, No. 1, pp. 5-20.
- Bulsara, V. N.; Talreja, R.; Qu, J.** (1999): Damage initiation under transverse loading of unidirectional composites with arbitrarily distributed fibers, *Comp. Sci. Tech*, vol. 59, pp. 673-682.
- Daniel, I. M.; Anastassopoulos, G.** (1995): Failure mechanisms and damage evolution in crossply ceramic-matrix composites, *Int. Jour. Solids Struct.*, vol. 32, pp. 341-355.

- Fish, J.; Wagiman, A.** (1993): Multiscale finite element method for a locally nonperiodic heterogeneous medium, *Comput. Mech.*, vol. 12, pp. 164-180.
- Garikipati, K.** (2002): A variational multiscale method to embed micromechanical surface laws in the macromechanical continuum formulation, *CMES: Computer Modeling in Engineering & Sciences*, vol. 3, no. 2, pp. 175-184.
- Ghoniem, N. M.; Cho, K.** (2002): The emerging role of multiscale modeling in nano- and micro-mechanics of materials, *CMES: Computer Modeling in Engineering & Sciences*, vol. 3, no. 2, pp. 147-174
- Ghosh, S.; Lee, K.; Raghavan, P.**, (2001): A multi-level computational model for multi-scale damage analysis in composite and porous materials, *Int. Jour. Solids Struct.* vol. 38, pp. 2335-2385.
- Ghosh, S.; Ling, Y.; Majumdar, B. S.; Kim R.** (2000): Interfacial debonding in multiple fiber-reinforced composites, *Mech. Mater.* vol. 32, no. 10, pp. 561 -591.
- Ghosh, S.; Mukhopadhyay, S.N.** (1991): A two dimensional automatic mesh generator for finite element analysis of random composites, *Comput. Struct.*, vol. 41, pp. 245-256.
- Ghosh, S.; Nowak, Z.; Lee, K.** (1997a): Tessellation based computational methods for the characterization and analysis of heterogeneous microstructures, *Comp. Sci. Tech.*, vol. 57, pp. 1187-1210.
- Ghosh, S.; Nowak, Z.; Lee, K.** (1997b): Quantitative characterization and modeling of composite microstructures by Voronoi cells, *Acta. Mat.*, vol. 45, pp. 2215-2234.
- Guedes, J.M.; Kikuchi, N.** (1991): Preprocessing and postprocessing for materials based on the homogenization method with adaptive finite element methods, *Comp. Meth. in Appl. Mech. Engng.*, vol. 83, pp. 143-198.
- Guo, B. Q.; Babuska, I.** (1986a): The  $h - p$  version of the finite element method. Part 1. The basic approximation results, *Comput. Mech.*, vol. 1, pp. 21-41.
- Guo, B. Q.; Babuska, I.** (1986b): The  $h - p$  version of the finite element method. Part 2. General results and applications, *Comput. Mech.*, vol. 1, pp. 203-226.
- Kwon, Y.W.; Roach, K.** (2004): Unit cell model of 2/2 twill woven fabric composites, *CMES: Computer Modeling in Engineering & Sciences*, Vol. 5, No. 1, pp. 63-72.
- Lee, K.; Moorthy, S.; Ghosh, S.** (1999): Multiple scale computational model for damage in composite materials, *Comp. Meth. Appl. Mech. and Engng.*, vol. 172, pp. 175-201.
- Moorthy, S.; Ghosh, S.** (1996): A model for analysis of arbitrary composite and porous microstructures with Voronoi cell finite elements, *Int. Jour. Numer. Meth. Engin.*, vol. 39, pp. 2363-2398.
- Moorthy, S.; Ghosh, S.** (1998): A Voronoi cell finite element model for particle cracking in composite materials, *Comp. Meth. Appl. Mech. Engin.*, vol. 151, pp. 377-400.
- Moorthy, S.; Ghosh, S.** (2000): Adaptivity and convergence in the Voronoi cell finite element model for analyzing heterogeneous materials, *Comp. Meth. Appl. Mech. Engng.*, vol. 185, pp. 37-74.
- Oden, J. T.; Zohdi, T. I.** (1997): Analysis and adaptive modeling of highly heterogeneous solids, *Comput. Meth. Appl. Mech. Engng.*, pp.3-25.
- Oden, J.T.; Vemaganti, K.; Moes, N.** (1999): Hierarchical modeling of heterogeneous solids, *Comput. Meth. Appl. Mech. Engng.*, vol. 172, pp. 3-25.
- Okada, H.; Fukui, Y.; Kumazawa, N.** (2004): Homogenization analysis for particulate composite materials using the boundary element method, *CMES: Computer Modeling in Engineering & Sciences*, Vol. 5, No. 2, pp. 135-149.
- Pagano, N.J.; Rybicki, E.F.** (1974): On the significance of effective modulus solutions for fibrous composites, *J. Comp. Mat.*, vol. 8, pp. 214-228.
- Pyrz, R.** (1994a): Quantitative description of the microstructure of composites. Part 1: Morphology of unidirectional composite systems, *Comp. Sci. Tech.*, vol. 50, pp. 197-208.
- Pyrz, R.** (1994b): Correlation of microstructure variability and local stress field in two-phase materials, *Mat. Sci. Eng.*, vol. A177, pp. 253-259.
- Raghavan, P.; Moorthy. S.; Ghosh, S.; Pagano, N. J.** (2001): Revisiting the composite laminate problem with an adaptive multi-level computational model, *Comp. Sci. Tech.*, vol. 61, pp. 1017-1040.
- Rybicki, E.F.; Pagano, N.J.** (1976): A study of the influence of microstructure on the modified effective modulus approach for composite laminates, *Proceedings of the 1975 Int. Conf. Compos. Matl.*, vol. 2, pp. 198-207.

**Sanchez-Palencia E.** (1980): Non-homogeneous media and vibration theory, *Lecture notes in Physics* No. 127, Springer-Verlag, Berlin Heidelberg.

**Zeman, J.; Sejnoha, M.** (2001): Numerical evaluation of effective elastic properties of graphite fiber tow impregnated by polymer matrix, *Jour. Mech. Phys. Solids*, vol. 49, pp. 69-90.